

# Minor embedding with Stuart-Landau oscillator networks

S. L. Harrison,<sup>1,\*</sup> H. Sigurdsson,<sup>2,1</sup> and P. G. Lagoudakis<sup>1,3</sup>

<sup>1</sup>*School of Physics and Astronomy, University of Southampton,  
Southampton, SO17 1BJ, United Kingdom*

<sup>2</sup>*Science Institute, University of Iceland,  
Dunhagi 3, IS-107, Reykjavik, Iceland*

<sup>3</sup>*Skolkovo Institute of Science and Technology Novaya St.,  
100, Skolkovo 143025, Russian Federation*

(Dated: June 12, 2025)

## Abstract

We theoretically implement a strategy from quantum computation to simulate Stuart-Landau oscillator dynamics in all-to-all connected networks, also referred as complete graphs. The technique builds upon the triad structure minor embedding which expands dense graphs of interconnected elements into sparse ones which can potentially be realised in future on-chip solid state technologies with tunable edge weights. Our analysis reveals that the minor embedding procedure allows simulating the XY model on complete graphs, thus bypassing a severe geometric constraint.

---

\*

## INTRODUCTION

Solving dense graph combinatorial optimisation problems has been studied thoroughly in the field of quantum annealing, where qubits and their relative coupling strengths represent graph vertices and edge weights respectively. To solve such problems using qubit networks, dense graphs are expanded to new graphs through the *minor embedding* technique in order to map an arbitrary graph problem to pre-existing qubit architectures [1–6]. In general, finding a valid minor embedding of an arbitrary graph with no assumption about the final embedding is an NP-hard problem [7] in itself, becoming more computationally heavy as the number of graph vertices increases [2]. However, a standardised minor embedding to the *triad structure* is commonly used, allowing any all-to-all graph to be mapped to a standard qubit architecture [1, 8, 9].

In this study, we minimise the classical XY Hamiltonian on randomly weighted complete graphs through dynamical annealing of dissipatively coupled Stuart-Landau oscillators minor embedded to a triad structure [1, 9]. Stuart-Landau networks can be represented as mathematical graphs with vertices corresponding to oscillators  $\psi_n = \rho_n e^{i\theta_n}$ , and weighted edges corresponding to the oscillator coupling strength. Recently, investigation has been devoted to the network dynamics of dissipatively coupled Stuart-Landau oscillators whose fixed point attractors correlate with minimal energy configurations of the XY Hamiltonian encoded in the network weights [10–12]. This opens up perspectives on analogue computing strategies based on oscillatory networks to heuristically solve a variety of complex graph problems such as the NP-hard max-3-cut problem [13], and the phase retrieval problem [14]. However, complex graph problems often require high degrees of graph connectivity. From a standard computer simulation perspective, this is not an issue [15, 16]. But when developing unconventional solvers e.g. optical computing platforms to solve them, taking advantage of photonic parallelism, ultrafast timescales, and low power consumption, many hurdles arise. We demonstrate how the minor embedding technique realises a more experimentally friendly strategy to simulate and study graph problems with high degrees of connectivity in dissipatively coupled oscillatory systems. These include polariton condensates [13, 17], photon condensates [18], non-degenerate optical parametric oscillators [19, 20], and coupled micro-laser arrays [21, 22].

As an example, when using planar microcavity polariton condensate systems [17, 23], the

coupling strength between neighbouring condensates decays exponentially with their spatial separation distance [24, 25], making the coupling beyond first nearest neighbours usually negligible. That, plus the need to control each inter-condensate coupling strength makes it nigh on impossible to solve an all-to-all connected graph beyond a handful of condensate vertices. We show that, these connectivity problems can, in principle, be overcome using the minor embedding technique to the triad structure, and the feasibility of the structure to simulate dynamics and emergent behaviour in all-to-all connected networks of nonlinear optical oscillators.

## THE STUART-LANDAU MODEL

The Stuart-Landau model describes a plethora of oscillatory systems and is formally derived from the normal form of an Andronov-Hopf bifurcation. We apply this universal model to describe the dynamics of our dissipatively coupled oscillators at the graph vertices written:

$$\dot{\psi}_n = -[i\omega_n + |\psi_n|^2] \psi_n + \sum_{m=1}^M J_{n,m} \psi_m \quad (1)$$

Here,  $\psi_n \in \mathbb{C}$  denotes the  $n$ th oscillator,  $\omega_n$  its intrinsic frequency, and  $J_{n,m}$  is the coupling strength between oscillator  $n$  and  $m$  corresponding to the weighted edge connecting graph vertices  $n$  and  $m$ . We can re-write the Stuart-Landau model in polar coordinates with  $\psi_n = \rho_n e^{i\theta_n}$  arriving at:

$$\dot{\rho}_n = -\rho_n^3 + \sum_m J_{n,m} \rho_n \rho_m \cos(\theta_m - \theta_n); \quad (2)$$

$$\dot{\theta}_n = \omega_n + \sum_m J_{n,m} \frac{\rho_m}{\rho_n} \sin(\theta_m - \theta_n). \quad (3)$$

It can be seen from the last term in Equation 3 that the phases of small amplitude oscillators are strongly affected by large amplitude oscillators. Notably, when the amplitudes of the oscillators are equal and static, Equation 3 describes the generalised *Kuramoto model* [26, 27]. In fact, in this limit where  $\rho_n = \rho_0$ , and  $\omega_n = 0$ , phase locked states of the Kuramoto network are described by the energy minima of the following Lyapunov potential [28],

$$\mathcal{L} = - \sum_{n,m} J_{n,m} \cos(\theta_n - \theta_m), \quad (4)$$

which is the same as the well known XY Hamiltonian. Therefore, the phase oscillators experience a gradient descent towards minima of the XY Hamiltonian  $\dot{\theta}_n = -\partial\mathcal{L}/\partial\theta_n$ . Naturally, there is no guarantee that the system will relax into a global minimum although, surprisingly, impressive results have been obtained numerically through direct numerical simulation of Stuart-Landau networks [11, 12].

## MINOR EMBEDDING

### A. Triad Graph

In the process of creating a triad graph, we must first consider the undirected complete graph (all-to-all connected graph) of  $N$  vertices  $K_N$ , with vertex set:  $V(K_N)$  and edge set:  $J(K_N)$ . Each vertex  $V_n$  is assigned an index  $n$  and each edge symmetrically connecting two distinct vertices  $V_n$  and  $V_m$  is denoted  $J_{n,m} = J_{m,n}$ . Through the process of minor embedding,  $K_N$  is mapped to the triad graph  $K_N^{\text{emb}}$  [shown for  $K_5$  in Figure 1(a,b)] by expanding each vertex  $V_n \in V(K_N)$  to a chain of uniform coupled vertices of length  $N - 1$ , with intra-chain edge weights set to,

$$J^{\text{intra}} = J_c, \quad (\text{coloured edges}). \quad (5)$$

Each vertex of the chain is adjacent to a single vertex of a another chain with inter-chain edge weights,

$$J_{n,m}^{\text{inter}} = J_{n,m}, \quad \forall J_{n,m} \in J(K_N), \quad (\text{black edges}). \quad (6)$$

Additional description can be found in [29].

Physically,  $J_c > 0$  gives precedence to in-phase locking between oscillators within each chain, which—in the context of spin Hamiltonians—can be regarded as ferromagnetic (FM) type coupling with the oscillator phasors  $\mathbf{s}_n = [\cos(\theta_n), \sin(\theta_n)]^T$  playing the role of two-dimensional spins. The aim of FM coupling is to minimise the deviation in the oscillator phases across each chain, in order to mimic the dynamics of the complete graph  $K_N$  [6]. In other words, the red vertex in the complete graph [red oscillator  $\psi_1$  in Figure 1(a)] is represented by the average amplitude and phase of the oscillators in the red chain of the triad [see grey solid box in Figure 1(b)]. Notice that the number of black edges in the complete graph is the same as in the triad graph.

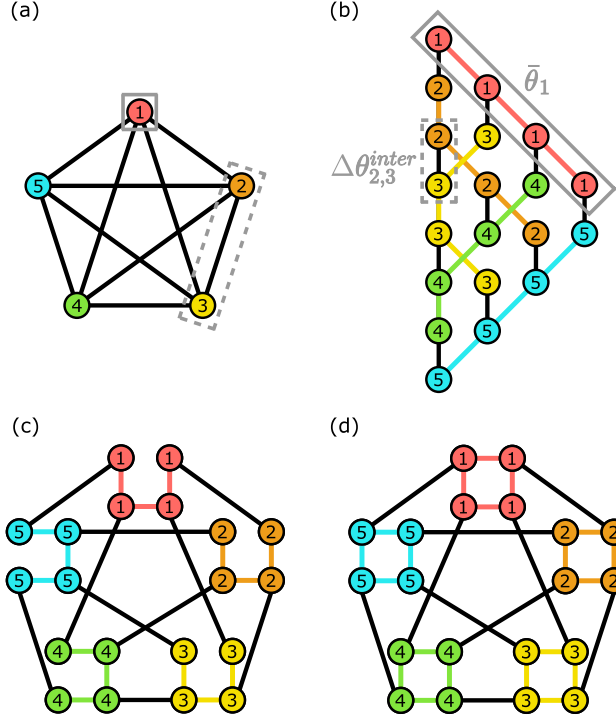


FIG. 1.

In this study, we will work close to the bifurcation threshold of the system separating the *normal state*  $\rho_n = 0$  from the oscillatory state  $\rho_n \neq 0$ , and are thus interested only in the phases of the oscillators whose average in each coloured chain is written,

$$\bar{\theta}_n = \frac{1}{N-1} \sum_{n' \in \text{chain}}^{N-1} \theta_{n,n'}. \quad (7)$$

We will refer to this phase averaging as *unembedding* the triad graph [30, 31]. That is, the averaged phases  $\bar{\theta}_n$  of the triad graph have been unembedded back to the vertices of the original complete graph.

Where the triad structure in Figure 1(b) is the hardware layout for investigating the minor embedding of complete graphs, it can be easier to picture the mapping process as the mathematical layout shown in Figure 1(c), where each vertex of  $K_N$  is expanded to a chain of length  $N-1$  about its original vertex site, such that the adjacency of the hardware layout [Figure 1(b)] and mathematical layout [Figure 1(c)] are equivalent.

We also consider the addition of an intra-chain edge between the first and last vertex of each chain [Figure 1(d)], thus “looping” them, such that the looped graph has a uniform degree of connectivity. Although this is more difficult to realise experimentally in

most platforms, we will compare results between unlooped and looped chains at minimising the XY Hamiltonian, and elucidate on how this more “symmetric” connectivity affects the performance of the triad graph.

## B. XY Energy Extraction

As mentioned above, each vertex of the complete graph  $K_N$  is associated with a complex valued number  $\psi_n$  containing information on the state the  $n$ th oscillator. We define the state vector of the graph as  $\boldsymbol{\psi} = [\psi_1, \psi_2, \dots, \psi_N]^T$  and its corresponding phase vector  $\boldsymbol{\theta} = [\theta_1, \theta_2, \dots, \theta_N]^T$ . The energy of the graph  $K_N$  is calculated from the XY Hamiltonian written,

$$H_{XY} = - \sum_{n,m}^N J_{n,m} \cos(\theta_n - \theta_m). \quad (8)$$

On the other hand, the energy of the triad graph can follow two methods. The first one defines the energy of the unembedded triad in the same way as Equation 8 but with the average phases across the chains  $\bar{\theta}_n$ ,

$$H_{XY}^{\text{unemb}} = - \sum_{n,m}^N J_{n,m} \cos(\bar{\theta}_n - \bar{\theta}_m). \quad (9)$$

We refer to this as the *unembedded energy* of the triad.

The other method directly uses the relative phase  $\Delta\theta_{n,m}^{\text{inter}}$  between all pairs of oscillators still “embedded” in the triad graph connected by a black inter-chain edge as depicted by the grey dashed boxes in Figure 1(a,b). We will refer to this as the *embedded energy* of the triad graph written,

$$H_{XY}^{\text{emb}} = - \sum_{n,m}^N J_{n,m} \cos(\Delta\theta_{n,m}^{\text{inter}}). \quad (10)$$

Note that when  $J_c = 0$  then minimising  $H_{XY}^{\text{emb}}$  is trivial since the graph forms just a set of  $N$  individual oscillator pairs connected by  $J_{n,m}$ .

## RESULTS

### Coherence Properties

Here, we numerically investigate and compare the phase coherence properties (i.e., the ability to synchronise in-phase) in the oscillator network dynamics between the complete

graph and the triad graph. We consider a complete FM graph where each oscillator is coupled equally to all the others with coupling strength  $J_{n,m} = J > 0$ . The frequencies  $\omega_n$  are randomly chosen from a normal distribution with density  $g(\omega)$  of mean  $\bar{\omega}$  and standard deviation  $\sigma$ . Naturally, we can always go into a rotating reference frame with frequency  $\bar{\omega}$  and therefore we can set  $\bar{\omega} = 0$  throughout our study without any loss of generality. We will use dimensionless units for all parameters and variables and fix  $\sigma = 1$  in this section. We point out that the oscillator coupling matrix  $\mathbf{J} = (J_{n,m}) \in \mathbb{R}^{M \times M}$  has always at least one positive eigenvalue for all graphs considered throughout the paper which means that the trivial  $\rho_n = 0$  solution is never stable. This means that the phases  $\theta_n(t)$  are well defined at all times when calculating the dynamics of [Equation 1](#).

To understand the emergent coherence properties of the network it is useful to define a phase order parameter, commonly used in analysis of such networks [\[28\]](#), to capture the degree of phase coherence between the oscillators. For the complete graph it is written,

$$r_{\text{complete}} = \frac{1}{N} \left| \sum_{n=1}^N e^{i\theta_n} \right|. \quad (11)$$

If all the oscillators have the same phase  $\theta_n = \theta_m$  then  $r_{\text{complete}} = 1$ , and in the limit of infinitely many uniform-randomly distributed phases on the interval  $[0, 2\pi)$  one has  $r_{\text{complete}} = 0$ .

We numerically integrate [Equation 1](#) from  $t = 0 \rightarrow T \gg J^{-1}, J_c^{-1}$  and calculate the average coherence  $\langle r_{\text{complete}} \rangle$  at the final time  $t = T$  over 160 random realisations of  $\omega_n$  and initial conditions (i.e., Monte Carlo sampling). We then repeat our calculation over a range of coupling strengths  $J$  [see [Figure 2\(a\)](#)] observing a gradual transition from an incoherent state to a coherent state with increasing coupling strength. This is reminiscent of the coherence bifurcation in Kuramoto networks [\[27, 28\]](#). There, all phase oscillators are in an incoherent state  $r_{\text{complete}} = 0$  below some critical coupling strength  $J_{\text{crit}}$  defined in the limit  $N \rightarrow \infty$ . As  $J$  is increased through and above  $J_{\text{crit}}$ , the system reaches a partially synchronised state  $r_{\text{complete}} > 0$ , where oscillators at the centre of  $g(0)$  are synchronised while those at the tails of the distribution remain in an incoherent state such that the system is split in two dynamical groups [\[32\]](#). As  $J$  is increased further, more oscillators join the synchronised group until the entire system becomes coherent [\[26, 33\]](#), as we observe with the Stuart-Landau model. Finite size effects can also be clearly observed in [Figure 2\(a\)](#) when changing the number of oscillators  $N$ . Notably, larger coupling strengths are needed

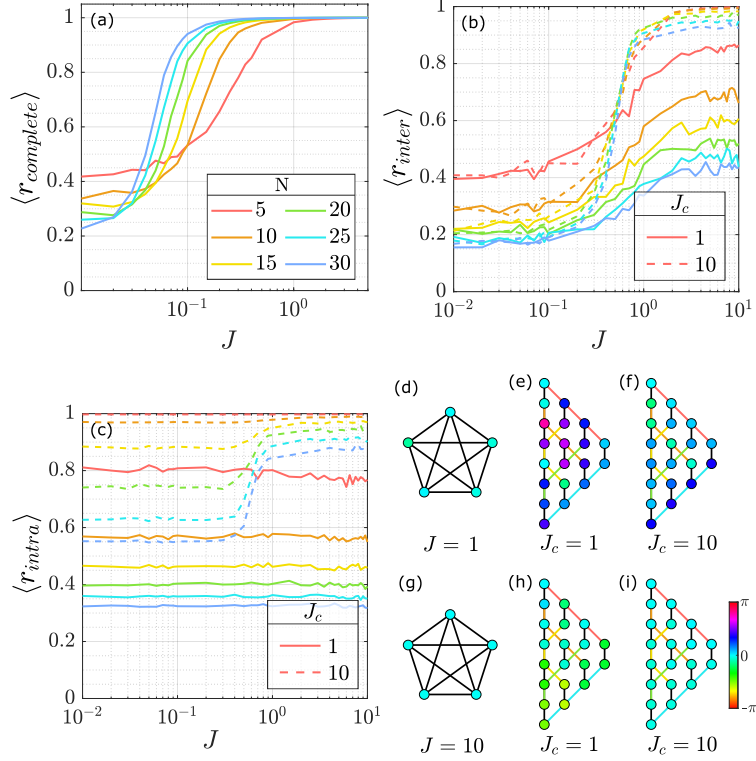


FIG. 2.

to synchronise smaller networks. We also point out that the presence of finite coherence values as  $J \rightarrow 0$  arises from these finite size effects which gradually decrease as  $N$  becomes larger.

We now move onto the triad graph. Similar to Equation 11, we can define coherence order parameters for the unembedded (averaged) phases of the triad graph,

$$r_{\text{inter}} = \frac{1}{N} \left| \sum_{n=1}^N e^{i\bar{\theta}_n} \right|, \quad (12)$$

and for the average phase coherence within each chain of the triad,

$$r_{\text{intra}} = \frac{1}{N} \sum_{n=1}^N \underbrace{\frac{1}{N-1} \left| \sum_{n' \in \text{chain}}^{N-1} e^{i\theta_{n,n'}} \right|}_{r_n^{\text{intra}}}. \quad (13)$$

For more details, please see Figure S1 in the Supplemental Material (SM). Just like for the complete graph, we average the coherences of the triad over 160 random samples of the dynamics denoted by  $\langle \cdot \rangle$ .

Considering two different orders of the scaling parameter  $J_c = \{1, 10\}$ , we investigate how the triad graph's coherence properties relate to the complete graph (going to lower and



larger orders of  $J_c$  did not qualitatively change the findings). Note that the frequencies  $\omega_n$  are randomly drawn from  $g(\omega)$  for all oscillators in the triad which represents experimental reality (i.e., we do not associate a single random frequency across each chain). As expected, when  $J_c$  is small the inter- and intra-chain coherences in Figure 2(b,c) show poor coherence with weak dependence on  $J$ . When  $J_c$  is large we instead observe a fast inter-chain coherence transition in Figure 2(b). This indicates that the triad graph managed to represent the embedded complete graph dynamics within  $J/J_c < 0.1$  which gives a figure of merit for the design requirements of possible triad graph platforms. Interestingly, in Figure 2(b) for large  $J$  the coherence is smaller in large graphs. This can be attributed to the fact that the chains within the triad graph need themselves to be coherent,  $r_{\text{intra}} \approx 1$ , in order to represent the embedded complete graph. But longer chains struggle more to settle on a phase and achieve good coherence as can be seen in Figure 2(c).

As both  $J$  and  $J_c$  increase, both inter and intra-chain coherences converge to unity and all oscillators synchronise. In Figure 2(d-i) we show example simulations of varying coupling strength where the vertex colours represent the steady state oscillator phases. The effect of looping the chains like shown in Figure 1(d) is found to have little effect on the coherence properties of the system (see Figure S2 in the Supplementary Material).

### XY Energy Minimisation

In this section we investigate the feasibility in using the minor embedding technique on complete graphs of Stuart-Landau oscillators to optimise the XY Hamiltonian. We compare the unembedded and embedded complete graph XY energies extracted from the triad structure [Equation 9,10] to the ground state of the XY Hamiltonian, as calculated using the classical basin hopping optimisation method [34]. Here we define the performance error of the Stuart-Landau system as the normalised difference in the extracted triad energies  $E_{tr}$  and the basin hopping energy  $E_{BH}$ ,

$$\text{Error} = \frac{E_{BH} - E_{tr}}{E_{BH}}. \quad (14)$$

Benchmarking is performed over 160 unique complete graphs with weights now randomly selected from a uniform distribution  $J_{n,m} \in [-1, 1]$  (there is no qualitative difference in using a normal distribution of same variance). To find the optimum embedding parameters, we

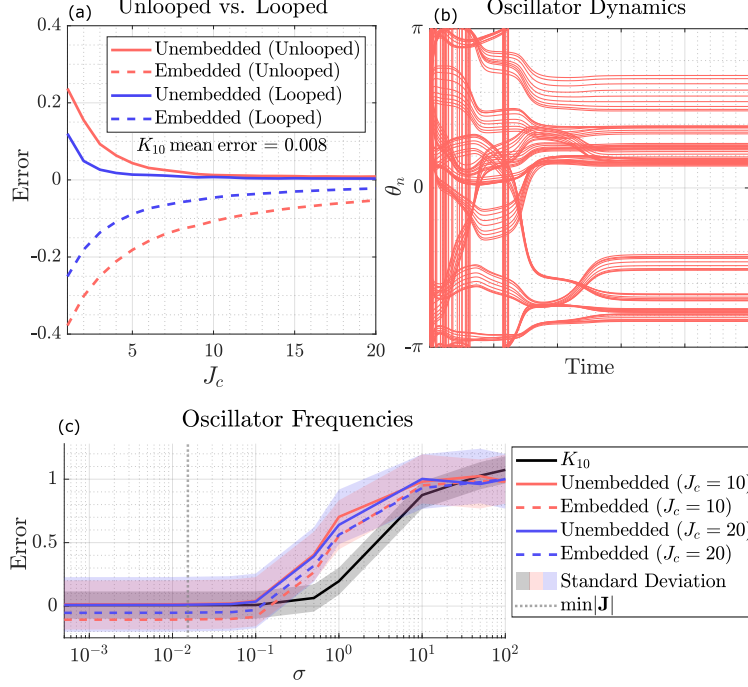


FIG. 3.

first consider  $N = 10$  using a range of  $J_c$  with unlooped and looped triad chains.

In Figure 3(a) we set  $\sigma = 0$  and see that the error of the extracted XY energies reduces as  $J_c$  is increased, where the unembedded XY energy converges to zero faster than the embedded energy, with a reduction in error for both methods when the triad chains are looped. This result is to be expected, as larger values of  $J_c$  reduce the distribution of phases across each triad chain, achieving a better representation of the complete graph in corroboration with Figure 2(b). This is seen in Figure 3(b) where the phase dynamics  $\theta_n(t)$  of the  $N(N - 1) = 90$  triad graph oscillators split into 10 moving paths, with each path representing a different triad chain. Interestingly, looping the chains in the considered case of  $N = 10$  oscillators is found to reduce their phase distribution (see Fig S2 in the Supplementary Material), achieving lower error. We point out that the negative error for the embedded XY energy stems from the fact that  $\min[H_{XY}^{\text{emb}}] < \min[H_{XY}]$  when  $J_c \rightarrow 0$ . In this limit, the triad graph breaks into  $N$  pair-coupled oscillators (only black edges remain) and the sum of their XY energies is trivially minimised by simply setting the relative phase in each pair to  $\Delta\theta_{n,m} = 0, \pi$  for positive and negative couplings, respectively.

When randomly distributed oscillator frequencies  $\omega_n$  are included ( $\sigma \neq 0$ ) in the dynamics we observe a fast increase in error with  $\sigma$  [see Figure 3(c)]. The frequencies  $\omega_n$  lead to

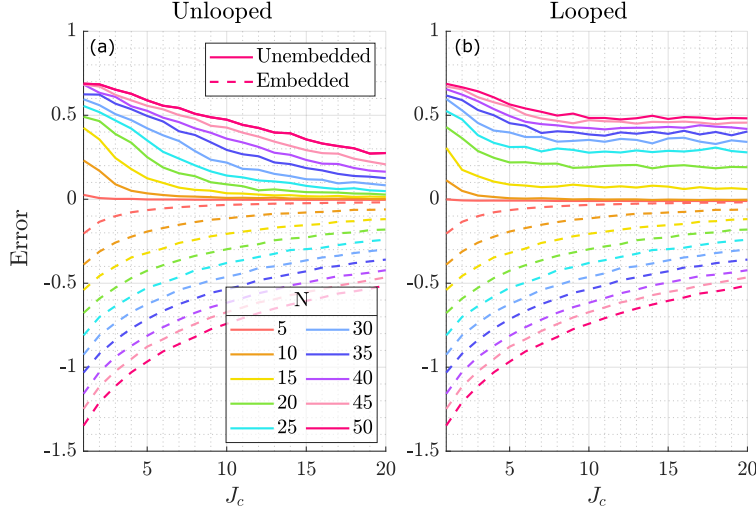


FIG. 4.

desynchronisation and the network steady state is lost with no well-defined phase relation that can enter into the XY Hamiltonian. This increase in error in the triad graph occurs for  $\frac{\sigma}{10} \gtrsim \min(J)$ . The XY energy of the complete and triad graphs are compared to the distribution of random phase configurations in Fig. S3. in the Supplementary Material.

Lastly, we show the performance of the triad graph as a function of both the problem (i.e., network) size  $N$  and  $J_c$  in Figure 4. As before, the error converges to zero with increasing  $J_c$  with better performance for the unembedded XY energy. As expected, larger networks struggle to find the correct (global) XY energy minimum and instead stabilise into the growing number of local minima. Interestingly, in Figure 4(b), when the chains are looped the unembedded XY energy error plateaus such that beyond  $J_c = 10$ , the embedded energy does not noticeably change and the benefit of looping the chains is only apparent for  $N \leq 10$ . This puzzling behaviour implies that looping the chains in the triad graph has generated a new family of stable attractors which do not correlate with the minima of the XY Hamiltonian. Such attractors could belong to twisted states in the chains which appear in sparse networks [35].

## CONCLUSIONS

We have demonstrated that the dynamics of an random all-to-all coupled Stuart-Landau oscillator network can be approximated using a minor embedding technique, regularly applied in the design of quantum computing platforms. Here, a complete (dense) graph is embedded into a sparse triad graph defined by a single embedding parameter  $J_c$ . We show that the steady-state phases in the embedded Stuart-Landau oscillator network can optimise its corresponding graph XY Hamiltonian, achieving good performance by simply adjusting its embedding parameter. The results are compared against the standard complete graph Stuart-Landau oscillator dynamics, and the classical Basin Hopping method.

The convergence of the minor embedded graph dynamics to that of the complete graph offers up the triad structure as a potential testbed for mapping out dense graph problems to continuous-phase coupled oscillator systems where fully-controllable all-to-all couplings are not practicable (such as polariton condensates, photonic condensates and coupled laser arrays). This opens perspectives on designing analogue computing hardware aimed at solving dense graphs problems (such as optimising the XY Hamiltonian) across a wide range of platforms in a similar spirit to quantum computing platforms.

- 
- [1] Choi, V. Minor-embedding in adiabatic quantum computation: II. Minor-universal graph design. *Quantum Inf Process* **10**, 343–353 (2011). URL <https://doi.org/10.1007/s11128-010-0200-3>.
  - [2] Cai, J., Mcready, W. G. & Roy, A. A practical heuristic for finding graph minors. *arXiv:1406.2741 [quant-ph]* (2014). URL <http://arxiv.org/abs/1406.2741>. ArXiv: 1406.2741.
  - [3] King, A. D. & McGeoch, C. C. Algorithm engineering for a quantum annealing platform. *arXiv:1410.2628 [quant-ph]* (2014). URL <http://arxiv.org/abs/1410.2628>. ArXiv: 1410.2628.
  - [4] Venturelli, D. *et al.* Quantum Optimization of Fully-Connected Spin Glasses. *Phys. Rev. X* **5**, 031040 (2015). URL <http://arxiv.org/abs/1406.7553>. ArXiv: 1406.7553.
  - [5] Perdomo-Ortiz, A. *et al.* Readiness of Quantum Optimization Machines for Industrial Appli-

- cations. *Phys. Rev. Applied* **12**, 014004 (2019). URL <https://link.aps.org/doi/10.1103/PhysRevApplied.12.014004>.
- [6] Hamerly, R. *et al.* Experimental investigation of performance differences between coherent Ising machines and a quantum annealer. *Science Advances* **5**, eaau0823 (2019). URL <https://advances.sciencemag.org/content/5/5/eaau0823>. Publisher: American Association for the Advancement of Science Section: Research Article.
  - [7] Zaribafiyani, A., Marchand, D. J. J. & Changiz Rezaei, S. S. Systematic and deterministic graph minor embedding for Cartesian products of graphs. *Quantum Inf Process* **16**, 136 (2017). URL <http://link.springer.com/10.1007/s11128-017-1569-z>.
  - [8] Choi, V. Minor-embedding in adiabatic quantum computation: I. The parameter setting problem. *Quantum Inf Process* **7**, 193–209 (2008). URL <https://doi.org/10.1007/s11128-008-0082-9>.
  - [9] Boothby, T., King, A. D. & Roy, A. Fast clique minor generation in Chimera qubit connectivity graphs. *Quantum Inf Process* **15**, 495–508 (2016). URL <http://link.springer.com/10.1007/s11128-015-1150-6>.
  - [10] Leleu, T., Yamamoto, Y., Utsunomiya, S. & Aihara, K. Combinatorial optimization using dynamical phase transitions in driven-dissipative systems. *Phys. Rev. E* **95**, 022118 (2017). URL <https://link.aps.org/doi/10.1103/PhysRevE.95.022118>.
  - [11] Kalinin, K. P. & Berloff, N. G. Global optimization of spin hamiltonians with gain-dissipative systems. *Scientific Reports* **8**, 17791 (2018). URL <https://doi.org/10.1038/s41598-018-35416-1>.
  - [12] Kalinin, K. P. & Berloff, N. G. Networks of non-equilibrium condensates for global optimization. *New Journal of Physics* **20**, 113023 (2018). URL <https://doi.org/10.1088/1367-2630/aae8ae>.
  - [13] Harrison, S. L., Sigurdsson, H. & Lagoudakis, P. G. Solving the max-3-cut problem using synchronized dissipative networks. *arXiv:2007.06135 [cond-mat, physics:quant-ph]* (2020). URL <http://arxiv.org/abs/2007.06135>. ArXiv: 2007.06135.
  - [14] Waldspurger, I., d’Aspremont, A. & Mallat, S. Phase recovery, maxcut and complex semidefinite programming. *Mathematical Programming* **149**, 47–81 (2015). URL <https://doi.org/10.1007/s10107-013-0738-9>.
  - [15] Goto, H., Tatsumura, K. & Dixon, A. R. Combinatorial optimization by simulating adiabatic

- bifurcations in nonlinear hamiltonian systems. *Science Advances* **5**, eaav2372 (2019).
- [16] Böhm, F., Vaerenbergh, T. V., Verschaffelt, G. & Van der Sande, G. Order-of-magnitude differences in computational performance of analog ising machines induced by the choice of nonlinearity. *Communications Physics* **4**, 149 (2021). URL <https://doi.org/10.1038/s42005-021-00655-8>.
  - [17] Berloff, N. G. *et al.* Realizing the classical XY Hamiltonian in polariton simulators. *Nature Mater* **16**, 1120–1126 (2017). URL <https://www.nature.com/articles/nmat4971>. Number: 11 Publisher: Nature Publishing Group.
  - [18] Vretenar, M., Kassenberg, B., Bissesar, S., Toebe, C. & Klaers, J. Controllable Josephson junction for photon Bose-Einstein condensates. *Phys. Rev. Research* **3**, 023167 (2021). URL <https://link.aps.org/doi/10.1103/PhysRevResearch.3.023167>. Publisher: American Physical Society.
  - [19] Tamate, S., Yamamoto, Y., Marandi, A., McMahon, P. & Utsunomiya, S. Simulating the classical xy model with a laser network (2016). 1608.00358.
  - [20] Takeda, Y. *et al.* Boltzmann sampling for an XY model using a non-degenerate optical parametric oscillator network. *Quantum Science and Technology* **3**, 014004 (2017). URL <https://doi.org/10.1088/2058-9565/aa923b>.
  - [21] Gershenzon, I. *et al.* Exact mapping between a laser network loss rate and the classical xy hamiltonian by laser loss control. *Nanophotonics* **9**, 4117–4126 (2020). URL <https://doi.org/10.1515/nanoph-2020-0137>.
  - [22] Reddy, A. N. K. *et al.* Phase-locking of lasers with Gaussian coupling. *arXiv:2106.02344 [physics]* (2021). URL <http://arxiv.org/abs/2106.02344>. ArXiv: 2106.02344.
  - [23] Kalinin, K. P., Amo, A., Bloch, J. & Berloff, N. G. Polaritonic xy-ising machine:. *Nanophotonics* **9**, 4127–4138 (2020). URL <https://doi.org/10.1515/nanoph-2020-0162>.
  - [24] Ohadi, H. *et al.* Nontrivial phase coupling in polariton multiplets. *Phys. Rev. X* **6**, 031032 (2016). URL <https://link.aps.org/doi/10.1103/PhysRevX.6.031032>.
  - [25] Harrison, S. L., Sigurdsson, H. & Lagoudakis, P. G. Synchronization in optically trapped polariton Stuart-Landau networks. *Phys. Rev. B* **101**, 155402 (2020). URL <https://link.aps.org/doi/10.1103/PhysRevB.101.155402>.
  - [26] Kuramoto, Y. Self-entrainment of a population of coupled non-linear oscillators. In Araki, H. (ed.) *International Symposium on Mathematical Problems in Theoretical Physics*, Lec-

- ture Notes in Physics, 420–422 (Springer, Berlin, Heidelberg, 1975). URL <https://link.springer.com/chapter/10.1007%2FBFb0013365>.
- [27] Strogatz, S. H. From Kuramoto to Crawford: exploring the onset of synchronization in populations of coupled oscillators. *Physica D: Nonlinear Phenomena* **143**, 1–20 (2000). URL <https://www.sciencedirect.com/science/article/pii/S0167278900000944>.
- [28] Acebrón, J. A., Bonilla, L. L., Pérez Vicente, C. J., Ritort, F. & Spigler, R. The Kuramoto model: A simple paradigm for synchronization phenomena. *Rev. Mod. Phys.* **77**, 137–185 (2005). URL <https://link.aps.org/doi/10.1103/RevModPhys.77.137>. Publisher: American Physical Society.
- [29] The resulting triad graph consists of vertex set:  $V_N^{\text{emb}}(K_N^{\text{emb}})$  containing  $N(N-1)$  vertices  $V_n^{\text{emb}}$ , and edge set:  $J_n^{\text{emb}}(K_N^{\text{emb}})$  containing  $\frac{N(N-1)}{2}$  inter-chain edges  $J_{n,m}^{\text{inter}}$  and  $N(N-2)$  intra-chain edges  $J_{n,m}^{\text{intra}}$ .
- [30] Pudenz, K. L. Parameter setting for quantum annealers. In *2016 IEEE High Performance Extreme Computing Conference (HPEC)*, 1–6 (2016).
- [31] Pelofske, E., Hahn, G. & Djidjev, H. Advanced unembedding techniques for quantum annealers. *arXiv:2009.05028 [quant-ph]* (2020). URL <http://arxiv.org/abs/2009.05028>. ArXiv: 2009.05028.
- [32] Strogatz, S. H. & Mirollo, R. E. Stability of incoherence in a population of coupled oscillators. *J Stat Phys* **63**, 613–635 (1991). URL <http://link.springer.com/10.1007/BF01029202>.
- [33] Kuramoto, Y. Chemical Oscillations, Waves, and Turbulence. Springer Series in Synergetics, 68–77 (Springer, Berlin, Heidelberg, 1984). URL [https://doi.org/10.1007/978-3-642-69689-3\\_5](https://doi.org/10.1007/978-3-642-69689-3_5).
- [34] Wales, D. J. & Doye, J. P. K. Global optimization by basin-hopping and the lowest energy structures of lennard-jones clusters containing up to 110 atoms. *The Journal of Physical Chemistry A* **101**, 5111–5116 (1997). URL <https://doi.org/10.1021/jp970984n>.
- [35] Townsend, A., Stillman, M. & Strogatz, S. H. Dense networks that do not synchronize and sparse ones that do. *Chaos: An Interdisciplinary Journal of Nonlinear Science* **30**, 083142 (2020). URL <https://doi.org/10.1063/5.0018322>.

## **ACKNOWLEDGEMENTS**

S.L.H., H.S., and P.G.L. acknowledge the support of the UK's Engineering and Physical Sciences Research Council (grant EP/M025330/1 on Hybrid Polaritonics) and S.L.H. acknowledges the use of the IRIDIS High Performance Computing Facility and associated support services at the University of Southampton. H.S. acknowledges the Icelandic Research Fund (Rannis), grant No. 217631-051.

## **AUTHOR CONTRIBUTIONS**

S.L.H. and H.S. contributed both to the theory and writing of the manuscript, S.L.H. oversaw numerical simulations, and P.G.L. lead the research and discussion throughout the project.

## **COMPETING INTERESTS**

The authors declare that they have no competing financial interests.

## **DATA AVAILABILITY**

All data supporting this article is available on the University of Southampton's online repository (DOI: tbc).



## FIGURE LEGENDS

**FIG. 1. Schematic of complete and triad graph structures.** (a)  $K_5$  graph mapped through minor embedding to (b) the  $K_5^{\text{emb}}$  triad graph, (c) the mathematical layout of  $K_5^{\text{emb}}$  and (d) when including  $N$  additional edges to loop the chains. In (b-d), the FM chain couplings are shown by coloured edges  $J^{\text{intra}} = J_c$  and the encoded coupling strength of  $K_5$  are shown by black edges, such that  $J_{n,m}^{\text{inter}} = J_{n,m}$ . The grey solid and dashed boxes overlayed on (a,b) demonstrate two possible phase extraction methods for the unembedded and embedded XY energies from the triad graph respectively.

**FIG. 2. Coherence across FM complete graph and corresponding triad graph.** Coherence of (a)  $\langle r_{\text{complete}} \rangle$  for uniform FM coupled complete graphs with coupling strength  $J$ , (b)  $\langle r_{\text{inter}} \rangle$  and (c)  $\langle r_{\text{intra}} \rangle$  for the corresponding triad graphs. All results are averaged over 160 instances of  $\omega_n$  and random initial conditions. Example steady state phases of  $N = 5$  oscillators in the (d,g) complete and triad structures with (e,h)  $J_c = 1$  and (f,i)  $J_c = 10$  for a single instance. (d-f)  $J = 1$  and (g-i)  $J = 10$ , where the phases are indicated by vertex colour.

**FIG. 3. Characterisation of triad graph XY energy dynamics.** (a) Error between the Stuart-Landau model and the classical-basin hopping method in minimising the XY Hamiltonian on a randomly connected complete graph with  $\sigma = 0$ . (b) The phase dynamics of the triad graph oscillators for a single random graph with  $J_c = 10$ . (c) Distribution of oscillator energies with unlooped triad chains and the complete graph, with translucent surfaces to represent the standard deviation in error of the unembedded energies and vertical lines to show the minimum magnitude in coupling strength across graphs (same units as  $\sigma$ ). Results in (a,c) are averaged over 160 random graphs and random initial conditions.

**FIG. 4. XY energy error of the minor embedded random complete graph.** XY energy error from the triad structure compared to the complete graph for (a) unlooped and (b) looped triad chains with  $N = 5$  to 50, averaged over 160 random graphs and  $\sigma = 0$ .

# Supplementary Material

## Minor embedding with Stuart-Landau oscillator networks

S. L. Harrison,<sup>1</sup> H. Sigurdsson,<sup>2,1</sup> and P. G. Lagoudakis<sup>1,3</sup>

<sup>1</sup>*School of Physics and Astronomy, University of Southampton, Southampton, SO17 1BJ, United Kingdom*

<sup>2</sup>*Science Institute, University of Iceland, Dunhagi 3, IS-107, Reykjavik, Iceland*

<sup>3</sup>*Skolkovo Institute of Science and Technology Novaya St., 100, Skolkovo 143025, Russian Federation*

(Dated: June 12, 2025)

### COHERENCE

#### A. Definitions

In the main text we extract the coherence across all oscillators in the complete graph  $r_{complete}$ , the coherence across the average phases of the chains  $r_{inter}$  and the average coherence across each chain  $r_{intra}$ . All three parameters are defined alongside a schematic in Fig. S1. Here,  $\theta_n$  is the phase of oscillator  $n$  in the complete graph,  $\theta_{n,n'}^{intra}$  is the phase of the  $n^{th}$  oscillator in triad chain  $n$  and  $\bar{\theta}_n$  is the average phase over the  $N - 1$  oscillators in chain  $n$ .

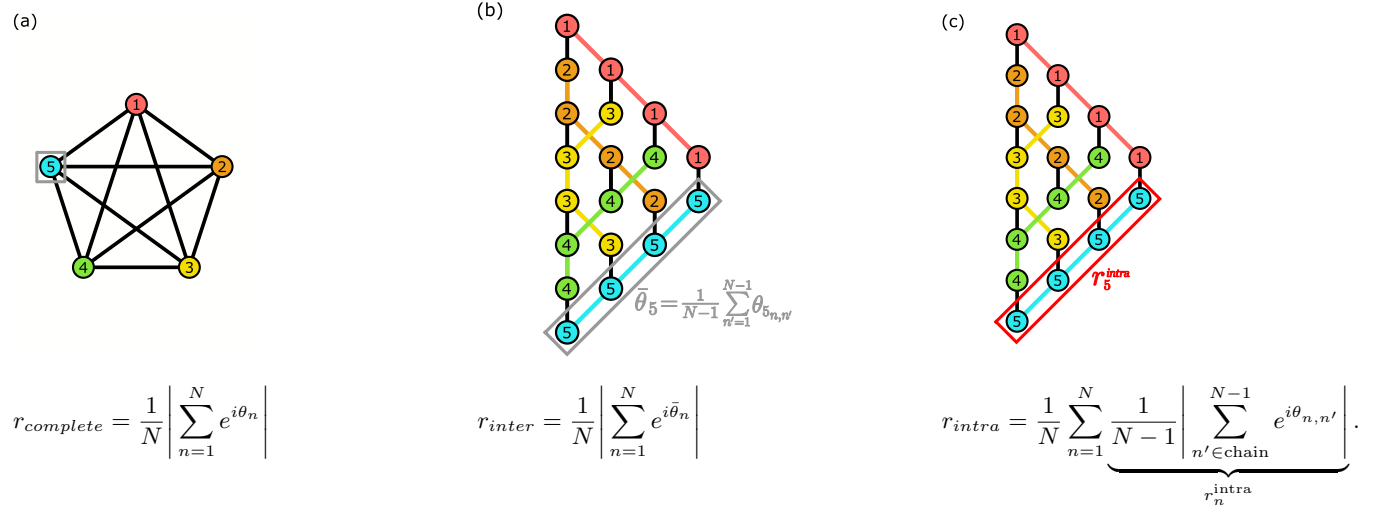


Fig. S1. (a) Coherence extracted over all oscillators in the complete graph, (b) the unembedded triad coherence between the  $N$  average chain phases, plus (c) the average chain coherence. All schematics represent the  $K_5$  and  $K_5^{emb}$  graphs with the grey boxes in (a,b) and red box in (c) representing the extraction of the average phase and coherence across chain 5 respectively.

#### B. Looping Triad Chains

In addition to the unlooped triad representation of the uniform FM complete graph in the main text, we also consider the effect of looping the triad chains on the coherence of the system under the same conditions as the unlooped case [Fig. S2]. When the minor embedded chains are looped, all oscillators are symmetrically coupled and thus the triad graph coherence is higher for the same coupling strength compared to the unlooped equivalent, as the edge effects of the unlooped chain coherence are eliminated. For  $J_c = 1$ ,  $r_{inter}$  and  $r_{intra}$  remain at a low coherence as the encoded complete graph weights are not dominant in the system. For  $J_c = 10$ , there is a coherence build up with increasing  $J$ , indicating that the triad coherence dynamics represent the complete graph for large  $J_c$ .

### RANDOM GRAPH XY ENERGY

We plot histograms of complete graph XY energies extracted from a random  $K_{10}$  graph for  $10^4$  random phase realisations alongside the extracted XY energies from the Stuart-Landau networks of  $K_{10}$  and  $K_{10}^{unemb}$ . As  $J_c$  increases,

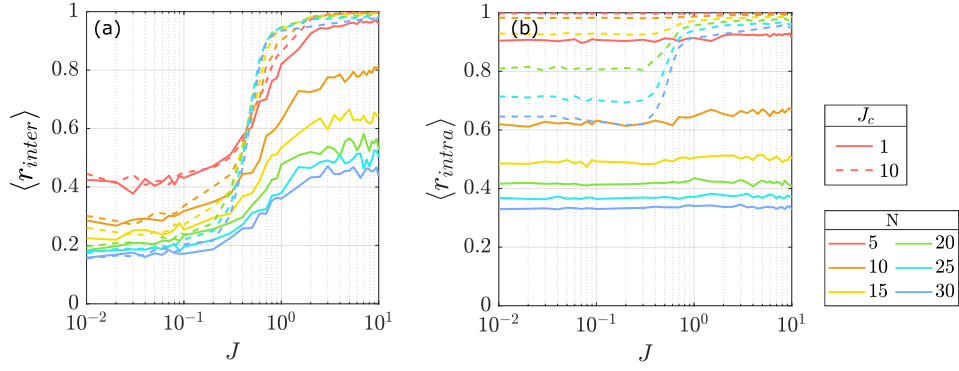


Fig. S2. Coherence (a)  $\langle r_{inter} \rangle$  and (b)  $\langle r_{intra} \rangle$  of triad graphs corresponding to uniform FM complete graphs with looped chains and  $J_c = 1$  and 10. All scanned over a range of coupling strengths  $J$  and averaged over 160 instances with standard deviation in oscillator frequencies  $\sigma = 1$ .

the unembedded and embedded energies converge to the complete graph energy [Fig. S3(a-d)], as we see in the main text and the energy of the triad graph is minimised for all  $J_c$  [Fig. S3(e-h)]. This confirms that the Stuart-Landau oscillator always minimises the XY Hamiltonian of the triad graph, but the ground state triad phase dynamics converge to those of the embedded complete graph when  $J_c$  is maximised.

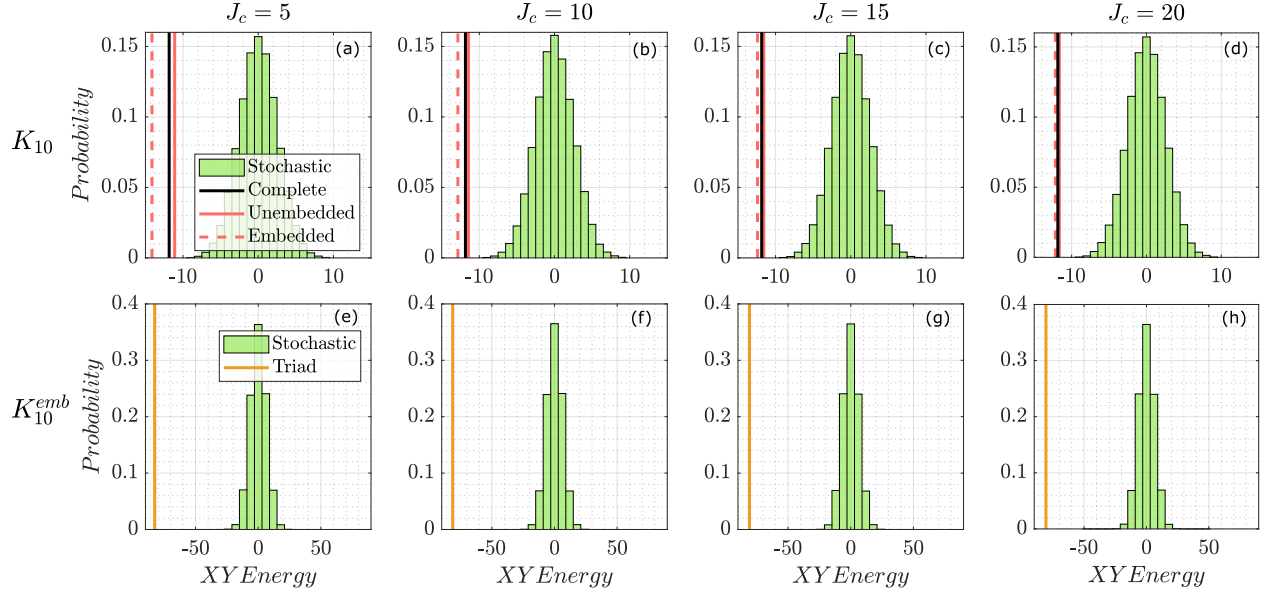


Fig. S3. (a-d) XY energy from a single random  $K_{10}$  graph and extracted embedded and unembedded energies from the corresponding triad graph compared to the XY energy from  $10^4$  random phase configurations. (e-h) XY energy of the  $K_{10}^{emb}$  graph compared to the XY energy of  $10^4$  random phase configurations. Each column representing  $J_c = 5, 10, 15$  and 20 respectively.